frontiers in Oncology

ORIGINAL RESEARCH
published: 27 November 2019
doi: 10.3389/fonc.2019.01297

# Evaluation of an Open Source Registration Package for Automatic Contour Propagation in Online Adaptive Intensity-Modulated Proton Therapy of Prostate Cancer

*Yuchuan Qiao[1], Thyrza Jagt[2], Mischa Hoogeman[2], Boudewijn P. F. Lelieveldt[1,3] and Marius Staring[1,3,4]**

[1] The Division of Image Processing, Department of Radiology, Leiden University Medical Center, Leiden, Netherlands, [2] Department of Radiation Oncology, Erasmus MC Cancer Institute, Rotterdam, Netherlands, [3] Intelligent Systems Department, Faculty of EEMCS, Delft University of Technology, Delft, Netherlands, [4] Department of Radiotherapy, Leiden University Medical Center, Leiden, Netherlands

OPEN ACCESS

**Edited by:**
Radka Stoyanova,
University of Miami, United States

**Reviewed by:**
Young Kwok,
University of Maryland Medical Center, United States
Eric Brooks,
University of Texas MD Anderson Cancer Center, United States

***Correspondence:**
Marius Staring
m.staring@lumc.nl

**Specialty section:**
This article was submitted to Radiation Oncology, a section of the journal Frontiers in Oncology

**Received:** 01 May 2019
**Accepted:** 08 November 2019
**Published:** 27 November 2019

**Citation:**
Qiao Y, Jagt T, Hoogeman M, Lelieveldt BPF and Staring M (2019) Evaluation of an Open Source Registration Package for Automatic Contour Propagation in Online Adaptive Intensity-Modulated Proton Therapy of Prostate Cancer. Front. Oncol. 9:1297. doi: 10.3389/fonc.2019.01297

**Objective:** Our goal was to investigate the performance of an open source deformable image registration package, `elastix`, for fast and robust contour propagation in the context of online-adaptive intensity-modulated proton therapy (IMPT) for prostate cancer.

**Methods:** A planning and 7–10 repeat CT scans were available of 18 prostate cancer patients. Automatic contour propagation of repeat CT scans was performed using `elastix` and compared with manual delineations in terms of geometric accuracy and runtime. Dosimetric accuracy was quantified by generating IMPT plans using the propagated contours expanded with a 2 mm (prostate) and 3.5 mm margin (seminal vesicles and lymph nodes) and calculating dosimetric coverage based on the manual delineation. A coverage of $V_{95\%} \geq 98\%$ (at least 98% of the target volumes receive at least 95% of the prescribed dose) was considered clinically acceptable.

**Results:** Contour propagation runtime varied between 3 and 30 s for different registration settings. For the fastest setting, 83 in 93 (89.2%), 73 in 93 (78.5%), and 91 in 93 (97.9%) registrations yielded clinically acceptable dosimetric coverage of the prostate, seminal vesicles, and lymph nodes, respectively. For the prostate, seminal vesicles, and lymph nodes the Dice Similarity Coefficient (DSC) was $0.87 \pm 0.05$, $0.63 \pm 0.18$, and $0.89 \pm 0.03$ and the mean surface distance (MSD) was $1.4 \pm 0.5$ mm, $2.0 \pm 1.2$ mm, and $1.5 \pm 0.4$ mm, respectively.

**Conclusion:** With a dosimetric success rate of 78.5–97.9%, this software may facilitate online adaptive IMPT of prostate cancer using a fast, free and open implementation.

**Keywords: intensity modulated proton therapy, image registration, open source software, `elastix`, prostate cancer**

# 1. INTRODUCTION

Intensity-modulated proton therapy (IMPT) for prostate cancer treatment has the potential to deliver a highly localized dose distribution to the target volume. However, IMPT is also sensitive to treatment-related uncertainties that may distort the planned dose distribution. These include uncertainties in patient set-up, inter-fraction and intra-fraction variations in the shape and position of the target volume and organs at risk (OARs), and uncertainties in the range of the proton beams (1–5).

The uncertainties are usually accounted in the clinical-target-volume to planning-target-volume (CTV-to-PTV) margin, while proton-therapy specific effects need to be accounted for by including robustness in the optimization of the treatment plan (2–4). Both come at a price in terms of sparing of OARs. Therefore, ideally, these uncertainties should be tackled at each treatment fraction by re-optimizing the treatment plan, based on a new CT scan-of-the-day. This requires new contours for the target and OARs. Manual re-contouring, however, takes a substantial amount of time, which would give rise to new shape and position uncertainties of the target and OARs. Fast automatic methods are therefore mandated.

Deformable Image Registration (DIR) provides an efficient way to automatically re-contour the repeat CT scan by establishing the spatial correspondence with the planning CT scan. The manual contours from the planning CT scan are then propagated to the repeat CT scan, thereby compensating for anatomical changes that may have occurred between the time of the acquisition of the planning CT scan and the time of delivery. In combination with fast IMPT treatment replanning this enables the reduction of margins and robust planning parameters. The important step of DIR in an online-adaptive IMPT procedure (re-contouring, re-planning, patient-specific QA), however, is currently rather time-consuming (6, 7) and DIR at the treatment delivery unit is time-critical and has high time-efficiency demands. In this paper we therefore developed and evaluated a fast and automatic DIR method, and performed a dosimetric evaluation for IMPT.

Many DIR algorithms implemented in commercial or open source software packages could be used clinically (8, 9). Commercial software packages are, however, frequently black boxes for users and have limited choices for parameter customization (6, 9). Open source packages are much more flexible and provide fully customizable algorithms (10–12). Moreover, they support the fundamental scientific principle of reproducibility, sharing of knowledge and thereby promote opportunities for scientific advancement (13–15).

Currently, most research focused on the validation of DIR for radiation therapy in terms of dose accumulation for the prostate (16–18) or other anatomical areas (19, 20), as well as in terms of the geometric accuracy (9, 21). Dosimetric or geometric validations were performed mostly independently or sometimes jointly, while the time cost of DIR was ignored. However, the time cost of image registration is also important for online adaptive IMPT (7, 10, 11). Kupelian et al. (22) found the prostate having a shift exceeding 5 mm in 15% of the fractions when duration exceeded 30 s and for some cases the motion was even larger than 10 mm when duration exceeded 240 s. Van der Wielen et al. (23) reported that the inter-fractional prostate motions not only have translational, but also rotational components and deformations. Moreover, if lymph nodes are included in the target volume then the differential motion of the prostate and lymph nodes have to be taken into account as well (24). Therefore, these deformations should be accounted for by DIR within a reasonable time span, especially when using a small margin like 3 mm (25). Conventional registration methods took from around 10 min to 1 h (26–29). Although recent advances in deep learning based image registration yield promise for real-time algorithms (30–32), this has not yet been shown for prostate CT radiotherapy. To our knowledge, the validation of open source packages on registration accuracy has not been investigated so far for prostate cancer in IMPT, in terms of the combination of geometric accuracy, dosimetric evaluation and runtime. The presented package, our software `elastix`, is open source and freely available for clinical application, research and further development. We compared its performance to another open source registration package: ANTs (https://github.com/ANTsX/ANTs) (33).

# 2. MATERIALS AND METHODS

## 2.1. Patients and Imaging

Eighteen patients treated for prostate cancer with intensity-modulated radiation therapy were included in this study (1, 3). All patients gave their consent before being enrolled in a phase II dose-escalation trial delivered with moderately hypo-fractionated pelvic IMRT at Haukeland University Hospital, Bergen, Norway. The trial had been approved by the local ethical committee before enrollment starting in 2007. The ethics committee is REC West, the western Norway regional committee for medical and health research ethics (number 2006-15727). A planning CT and 7–10 repeat CTs evenly distributed throughout their treatment course were acquired out-of-room for each patient using a Philips Brilliance Big Bore CT scanner and anonymized with DicomWorks (Software Version: 2.2.1). The prostate, seminal vesicles, lymph nodes, and main OARs (rectum and bladder) of all patients were within the field-of-view. Geometric evaluation of DIR was performed using all images, while dosimetric evaluation was performed on a subset of 11 patients for which manual delineations of the bowels and femoral heads were available (needed for treatment planning). Each CT scan contained 90–180 slices and were reconstructed with a slice thickness of 2-3 mm. Each slice was of size 512 × 512 pixels and had an in-slice pixel resolution in the range from 0.84 × 0.84 mm to 0.95 × 0.95 mm. Golden fiducial markers (2 to 3) were implanted in the prostate for daily set-up to ensure an accurate alignment of the target with the treatment beams (34).

For each CT scan, the prostate, seminal vesicles, lymph nodes, bladder and rectum were delineated by an expert, and independently reviewed by another expert (1). The original images and delineations are in DICOM-RT format and were converted to meta image format and VTK meshes using MevisLab (http://www.mevislab.de/).

## 2.2. Image Registration

In this study, deformable image registration was performed using the open source software package `elastix` (12). This software is freely available from http://elastix.isi.uu.nl under the liberal Apache 2.0 license. All experiments were performed on a workstation with 64 GB memory, Linux system and an Intel Genuine i7-6850K CPU with 12 cores running at 3.6 GHz, utilizing only the CPU, without GPU acceleration.

For each patient, the planning CT scan (moving image) was registered to the repeat CT scans (fixed image), and then the manual delineations were propagated from the planning CT scan based on the corresponding deformations generated by DIR. The detailed procedure is as follows:

1. Preprocessing: A mask of the torso was generated automatically using in-house software Pulmo (commercialized by Medis specials, Leiden, The Netherlands), to eliminate the influence of the couch on image registration quality (35), and it was used for cropping the images. Each original image was cropped around the torso mask, using a 2 voxel margin, to further accelerate DIR. This preprocessing took much less than 1 s and is excluded in the runtime measures reported below.
2. Image registration: Image registrations were initialized based on the centers of gravity of the bony anatomy (tissue with HU > 200) of the cropped fixed and moving image. Then an affine registration was applied to tackle large movements of the organs, followed by DIR to compensate for local deformations. Image registration is formulated as an optimization problem:

$$\widehat{\boldsymbol{\mu}} = \arg\min_{\boldsymbol{\mu}} \mathcal{C}(I_F, I_M \circ \boldsymbol{T}(\boldsymbol{x}, \boldsymbol{\mu})), \tag{1}$$

where $I_F$ and $I_M$ are the fixed and moving image, respectively, $\boldsymbol{x}$ is an image voxel location and $\boldsymbol{T}(\boldsymbol{x}, \boldsymbol{\mu})$ is a coordinate transformation parameterized by $\boldsymbol{\mu}$. In this paper, an accelerated version of adaptive stochastic gradient descent (36) was used for iterative optimization of Equation (1). The number of iterations was varied between 100, 500, 1,000, and 2,000 iterations per resolution in the experiments below, in order to inspect the relation between DIR quality and runtime. A B-spline transformation model (37) was chosen and a fast recursive implementation was used (38). With the recursive B-spline, the original B-spline interpolation at a spatial coordinate $\boldsymbol{x} \in R^D$,

$$\boldsymbol{u}(\boldsymbol{x}) = \sum_{\boldsymbol{k} \in Z^n(\boldsymbol{x})} \boldsymbol{B}^n(\boldsymbol{x} - \boldsymbol{k}) \boldsymbol{\mu}(\boldsymbol{k}), \tag{2}$$

can be rewritten as:

$$\boldsymbol{u}(\boldsymbol{x}) = \sum_{\boldsymbol{k}_1 \in Z^n(\boldsymbol{x}_1)} \beta^n(\boldsymbol{x}_1 - \boldsymbol{k}_1) \sum_{\boldsymbol{k}_2 \in Z^n(\boldsymbol{x}_2)} \beta^n(\boldsymbol{x}_2 - \boldsymbol{k}_2) \cdots \sum_{\boldsymbol{k}_D \in Z^n(\boldsymbol{x})} \beta^n(\boldsymbol{x}_D - \boldsymbol{k}_D) \boldsymbol{\mu}(\boldsymbol{k}), \tag{3}$$

where $\boldsymbol{B}^n(\cdot)$ is the multi-dimensional B-spline polynomial of order $n$, $Z^n(\cdot)$ is its support region, $\boldsymbol{k}$ is the multi-dimensional index, $\boldsymbol{\mu}(\boldsymbol{k})$ are the control point coefficients, and $D$ is the image dimension. Here, we took advantage of the separability property of the B-spline leading to less computations. Equation (3) can be computed in a recursive manner, see the paper (38). Template Meta Programming, which is a programming paradigm to enable the compiler to generate efficient assembly code, was used to implement the recursive formulation of the B-spline transformation. This resulted in approximately 2 times faster registration performance than the default implementation (38). We used mutual information as a similarity measure (39). Multi-threading and parallellization of parts of the software in combination with further software optimization were applied to the software for further acceleration. A three level multi-resolution scheme was chosen to deal with local minima and to reduce calculation burden: the images were smoothed using a Gaussian filter with standard deviations of 2, 1, and 0.5 mm. Detailed parameter settings are available at the `elastix` parameter file database found at the `elastix` website.
3. Automatic contour propagation: After image registration, the deformation field generated from the previous step was applied to the manual delineations of the planning scan to generate a new contour of the scan of the day. This step took substantially less than 1 s and was also excluded from the runtime measures reported below.

Standard practice in image-guided radiotherapy is to use implanted intra-prostatic markers for daily patient alignment. Therefore, the proposed DIR approach will be compared to this default strategy, i.e., marker based translation, MBT in short.

Registration with this procedure was compared with another state-of-the-art open source registration tool: ANTs. As ANTs is widely used in multimodality neuroimaging registration (40) and lung CT image registration (41), it is also applied to head and neck proton therapy (42), radiation therapy on primary tumor vasculature (43) and prostate cancer radiation therapy (44). We compared the proposed method to the latest release of ANTs (v2.3.1) on the same machine with the same preprocessing scheme as detailed above. Mutual information is chosen as a dissimilarity measure with 32 as the number of bins for computing mutual information. Random sampling is applied, using 25% of all voxels to compute the dissimilarity measure. The deformation field is modeled with the diffeomorphic BSplineSyN model with a grid size of 0.3. For 3 resolutions, the number of iterations is set to 80, 80, and 60, respectively. The smoothing and shrinking factors are set to $3 \times 2 \times 1$ and $4 \times 2 \times 1$, respectively. These parameters are derived from Cao et al. (44) and manually tuned a lot for prostate CT image registration.

## 2.3. Evaluation Measurements

For quantitative evaluation of the automatic DIR method we considered several aspects, such as runtime, recontouring quality and dosimetric coverage. Runtime is measured by the system clock, in seconds. The recontouring quality of the prostate, seminal vesicles, lymph nodes, bladder and rectum is measured by comparing the automatically propagated contour from the planning CT scan with the manual delineation of the repeat CT scan. As a first measure we consider the Dice Similarity

Coefficient (DSC) (45):

$$\mathrm{DSC} = \frac{2|\boldsymbol{R_M} \cap \boldsymbol{R_F}|}{|\boldsymbol{R_M}| + |\boldsymbol{R_F}|}, \quad (4)$$

where $\boldsymbol{R_F}$ and $\boldsymbol{R_M}$ are the manually delineated regions in the repeat CT scan image and the propagated region in the planning CT scan image, respectively.

Two types of symmetric surface distances are used, namely the mean surface distance (MSD) and the 95% percentile Hausdorff distance (95%HD). Let $\boldsymbol{F} = \{a_1, a_2, \ldots, a_n\}$, and $\boldsymbol{M} = \{b_1, b_2, \ldots, b_m\}$ represent the mesh points from two surfaces, their definitions are as follows (46):

$$\mathrm{MSD} = \frac{1}{2}\left(\frac{1}{n}\sum_{i=1}^{n} d(a_i, \boldsymbol{M}) + \frac{1}{m}\sum_{i=1}^{m} d(b_i, \boldsymbol{F})\right), \quad (5)$$

$$95\%\mathrm{HD} = \max\left\{\mathrm{PERC95}(d(a_i, \boldsymbol{M})), \mathrm{PERC95}(d(b_i, \boldsymbol{F}))\right\}, \quad (6)$$

in which $d(a_i, \boldsymbol{M}) = \min_j \|b_j - a_i\|$. Both distances are computed in 3D. The geometrical success rate $\gamma$ is defined as the percentage of registrations which has a MSD $< 2$ mm (slice thickness) for the prostate: $\gamma = n\{\mathrm{MSD} < 2\,\mathrm{mm}\}/N$, where $N = 159$ is the total number of registrations.

To measure the dosimetric impact of differences in manual delineations and automatically re-contoured delineations, IMPT plans were generated on each repeat CT scan for both sets of delineations (manual and automatic) for the 11 patients where delineations of the femoral heads and bowels are available. To evaluate the difference between the two delineations and the effect these differences have on the dose distributions, both IMPT plans are evaluated on the manual contours, which therefore acts as the ground truth. All IMPT plans were generated using Erasmus-iCycle, an in-house developed treatment planning system (47, 48). Erasmus-iCycle uses a multi-criteria optimization to generate a clinically desirable Pareto optimal treatment plan on the basis of a wishlist consisting of hard constraints and objectives. A small margin is used (2 mm around the prostate and 3.5 mm around the seminal vesicles and lymph nodes) to compensate for inevitable inaccuracies of the contour-propagation and to account for intra-observer variations in the manual contouring. Note that without the envisioned online-adaptive approach the margins are far from sufficient to account for shape and positions changes of the target volume, for which clinically a margin of 7 mm is used (3, 49, 50). Dose was prescribed according to a simultaneously integrated boost scheme in which the high-dose target volume (prostate + 2 mm margin) was assigned 74 Gy and the low-dose target volume (lymph nodes and seminal vesicles + 3.5 mm margin) 55 Gy, to be delivered using two laterally opposed beams. The optimization ensures that at least 98% of the target volumes receive at least 95% of the prescribed dose ($V_{95\%} \geq 98\%$). To avoid overdose the optimization ensures that less than 2% of the target volumes receive more than 107% of the highest prescribed dose ($V_{107\%} \leq 2\%$). Target dose conformity and low dose to the OARs was achieved by including artificial rings around the target and including OARs in the wishlist (51). For the recontouring to be clinically acceptable the automatically generated treatment plans should still fulfill these criteria. Plans from automatic recontouring are therefore evaluated based on the manual contours. The clinical success rate $\eta$ is defined as the percentage of registrations for which the prostate directly meets the dose treatment criteria: $\eta = n\{V_{95\%} \geq 98\%\}/N, N = 93$. A second more conservative measure of clinical success is when all target volumes (the prostate, seminal vesicles and lymph nodes) meet this dosimetric criterium: CSR $= n\{(V_{95\%} \geq 98\%)_{\mathrm{Prostate}}$ AND $(V_{95\%} \geq 98\%)_{\mathrm{SV}}$ AND $(V_{95\%} \geq 98\%)_{\mathrm{LN}}\}/N, N = 93$, where SV is seminal vesicles and LN is lymph nodes, respectively.

# 3. RESULTS

## 3.1. Image Registration Performance

Examples of automatically propagated contours using DIR are given in **Figure 1**. **Table 1** presents the overlap after DIR for different numbers of iterations. For the prostate, we obtained a DSC of $0.88 \pm 0.03$ for each patient and all settings, and a similar overlap for the lymph nodes. The most difficult structures are the seminal vesicles, which have small volume and only achieved an overlap of $0.66 \pm 0.16$ for 100 iterations, and $0.67 \pm 0.13$ when the number of iteration is at least 500. For the OARs, we obtained a DSC of $0.77 \pm 0.07$ for the rectum and $0.88 \pm 0.09$ for the bladder for 100 iterations, and small improvements are observed when the number of iterations increased to at least 500. DSC scores generally improved from 100 to 500 iterations, but not after that. Compared to MBT we observe a 20% increase in DSC of seminal vesicles when using the proposed DIR method.

The mean surface distance (MSD) between the propagated and manually delineated contours are shown in **Table 2**. Note that for an increasing number of iterations the MSD slightly increased for the prostate and lymph nodes, likely due to the reduction in MSD of the bladder, rectum and seminal vesicles. However, also note that the MSD of the target organs were smaller than 1.8 mm which was within one voxel ($0.9 \times 0.9 \times 2$ mm). The 95% Hausdorff distance between the propagated and manual contour is shown in **Table 3**, which shows a similar pattern as the MSD. The geometrical success rate of the registrations was 96% (153 in 159) for DIR using 100 iterations and 96% (152 in 159) for DIR using more iterations, while this value was 77% (122 in 159) for affine registration. From **Figure 2**, we can see that DIR improved substantially compared to MBT, especially for the seminal vesicles, rectum and bladder.

The total runtime in seconds for each registration setting was $3.1 \pm 0.2$, $8.8 \pm 0.2$, $16.1 \pm 0.4$ and $30.5 \pm 0.4$ s, for 100, 500, 1,000, and 2,000 iterations, respectively. **Figure 3** illustrates the registration accuracy with respect to the mean runtime for different anatomical structures. Boxplots of the Dice overlap, mean surface distance and 95% Hausdorff distance are shown for all registrations ($N = 159$).

The geometric results of ANTs are presented in **Table 4** and **Figure 4**. The results shown in **Table 4** present the geometric measures for each organ. It shows `elastix` outperformed ANTs for all different measures at different anatomical structures except for a 0.01 DSC difference for the lymph nodes. The runtime is about $10^3$ times faster for `elastix` compared to

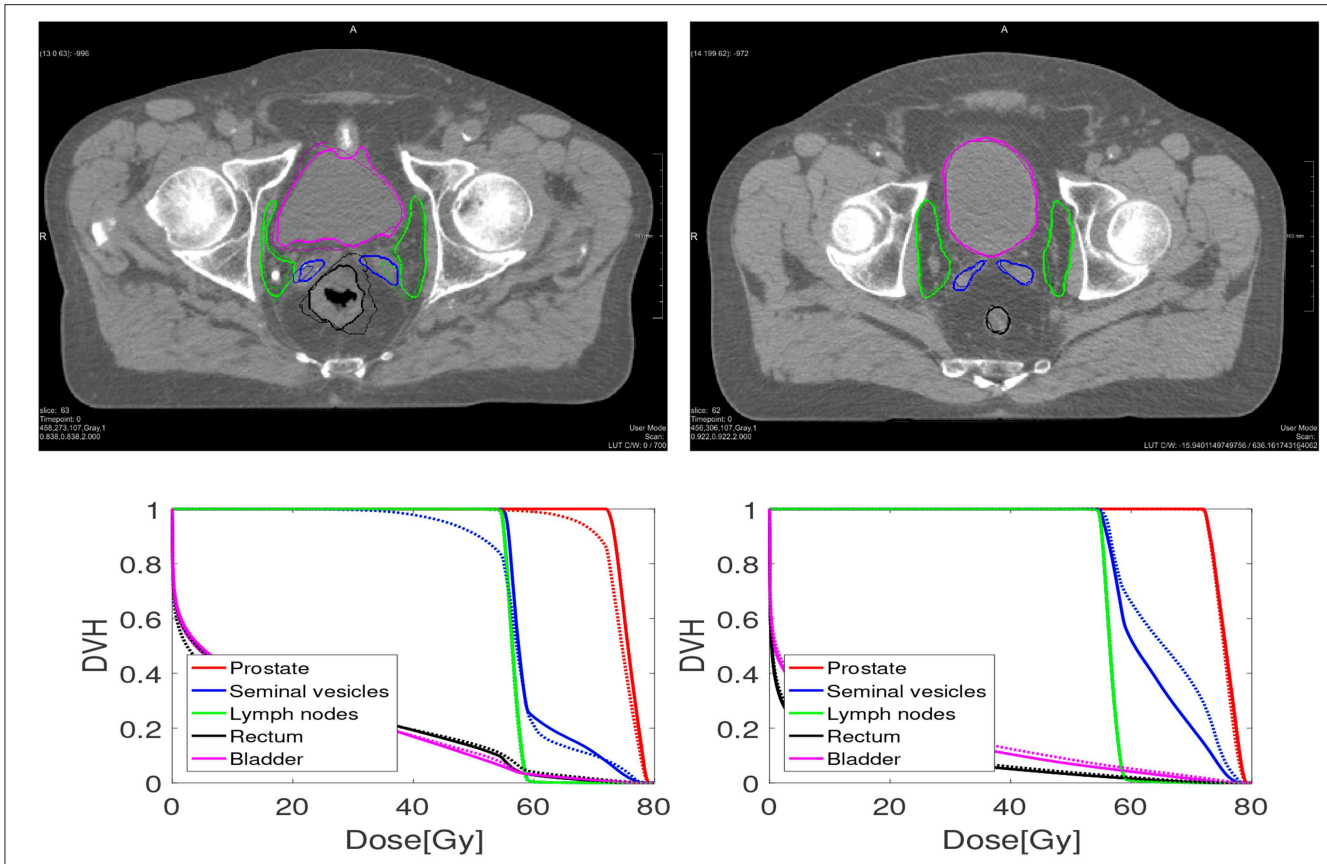


**FIGURE 1 |** An example of one case **(Left)** where the dosimetric criteria was met for `elastix`, and one case **(Right)** where not. The bottom figures are dose volume histograms. The solid line represents the manual contouring results while the dotted line is the automatically propagated one with the setting of 100 iterations. For the prostate (left and right), the MSD is 2.26 and 1.12 mm, while $V_{95\%}$ is 90.8% and 99.8%, respectively. For the seminal vesicles **(Left, Right)**, the MSD is 2.74 and 1.00 mm, while $V_{95\%}$ is 88% and 100%, respectively. For the lymph nodes **(Left, Right)**, the MSD is 1.45 and 0.99 mm, respectively, while $V_{95\%}$ both are 100%.

**TABLE 1 |** Dice overlap of different organs for different `elastix` registration settings.

| | Prostate | Seminal vesicles | Lymph nodes | Rectum | Bladder |
|---|---|---|---|---|---|
| **Nr. it.** | **Mean ± std** | **Mean ± std** | **Mean ± std** | **Mean ± std** | **Mean ± std** |
| MBT | 0.88 ± 0.03 | 0.55 ± 0.21 | 0.86 ± 0.05 | 0.71 ± 0.08 | 0.78 ± 0.09 |
| Affine | 0.85 ± 0.08 | 0.46 ± 0.25 | 0.90 ± 0.04 | 0.71 ± 0.08 | 0.78 ± 0.09 |
| 100 | 0.87 ± 0.05 | 0.63 ± 0.18 | 0.89 ± 0.03 | 0.76 ± 0.06 | 0.86 ± 0.09 |
| 500 | 0.87 ± 0.05 | 0.64 ± 0.17 | 0.88 ± 0.03 | 0.77 ± 0.06 | 0.87 ± 0.09 |
| 1,000 | 0.87 ± 0.05 | 0.64 ± 0.17 | 0.88 ± 0.03 | 0.77 ± 0.06 | 0.87 ± 0.09 |
| 2,000 | 0.87 ± 0.05 | 0.65 ± 0.16 | 0.88 ± 0.03 | 0.78 ± 0.06 | 0.88 ± 0.10 |

**TABLE 2 |** Mean surface distance (mm) of different organs for different `elastix` registration settings.

| | Prostate | Seminal vesicles | Lymph nodes | Rectum | Bladder |
|---|---|---|---|---|---|
| **Nr. it.** | **Mean ± std** | **Mean ± std** | **Mean ± std** | **Mean ± std** | **Mean ± std** |
| MBT | 1.36 ± 0.31 | 2.29 ± 1.10 | 1.76 ± 0.59 | 3.82 ± 1.41 | 4.40 ± 2.13 |
| Affine | 1.68 ± 0.85 | 2.98 ± 1.82 | 1.30 ± 0.48 | 3.95 ± 1.46 | 4.45 ± 2.11 |
| 100 | 1.42 ± 0.48 | 1.97 ± 1.22 | 1.46 ± 0.44 | 3.29 ± 1.31 | 2.92 ± 1.90 |
| 500 | 1.42 ± 0.48 | 1.90 ± 1.19 | 1.50 ± 0.44 | 3.20 ± 1.27 | 2.61 ± 1.81 |
| 1,000 | 1.42 ± 0.46 | 1.88 ± 1.16 | 1.53 ± 0.43 | 3.15 ± 1.27 | 2.47 ± 1.73 |
| 2,000 | 1.43 ± 0.49 | 1.87 ± 1.16 | 1.55 ± 0.43 | 3.10 ± 1.27 | 2.35 ± 1.67 |

ANTs (3,659 ± 2,747 s). Runtime of ANTs is majorly influenced by the parameter settings, especially by the grid size. Larger grid size needs less runtime for ANTs, however, the accuracy will be sacrificed. The boxplots of the difference of each measure between `elastix` and ANTs are given in **Figure 4**. All results show statistical difference when using a Wilcoxon signed-rank test at $p = 0.05$.

## 3.2. Dosimetric Validation

All treatment plans from `elastix` were evaluated by visual inspection of the dose distributions, the dose-volume histograms (DVHs) of the target volumes and OARs, and the clinical constraints. For the prostate, seminal vesicles and lymph nodes, we report the $V_{95\%}$ and $V_{107\%}$ of each treatment plan that used the DIR-generated contours. For the rectum, we consider $V_{45Gy}$,

$V_{60Gy}$, $V_{75Gy}$, and $D_{mean}$, while for the bladder $V_{45Gy}$, $V_{65Gy}$ and $D_{mean}$ are used, where $D_{mean}$ means the average dose to the structure.

**Figure 5** shows a boxplot depicting the difference in dosimetric parameters between the automatically generated delineations (100 iterations setting) and the manual delineations, in the treatment plan that was based on the automatically generated delineations. We can see that for all dosimetric parameters the median of the differences are close to 0. However, there are some scans for which larger differences occur for especially the $V_{95\%}$ of the seminal vesicles.

**Table 5** shows the percentage of scans for which $V_{95\%} \geq 98\%$ and $V_{107\%} \leq 2\%$ for the treatment plans based on the automatically contoured structures. Note that the success rate when using the manual delineations is close to 100% for all organs. As one can see, DIR using 100 iterations obtained a success rate of 89.2% for the prostate and 78.5% for the seminal vesicles, and these numbers are improved to 89.2% and 88.2%, respectively for 500 iterations. The conservative success rate based on all three target volumes increased from 68.8% to 77.4%, for 100 and 500 iterations, respectively. For MBT, the CSR was only 50%, meaning that in 50% of the cases manual interaction during quality control is warranted. Compared to MBT, DIR improved the success rates with 9.4%, 26.6%, and 8.5% for the prostate, seminal vesicles, and lymph nodes, respectively. The CSR improved as much as 57% when using 1,000 iterations. From **Figure 6**, we can observe the improvements of DIR using 100

**TABLE 3 |** 95% percentile Hausdorff distance (mm) of different organs for different `elastix` registration settings.

| | Prostate | Seminal vesicles | Lymph nodes | Rectum | Bladder |
|---|---|---|---|---|---|
| **Nr. it.** | **Mean ± std** | **Mean ± std** | **Mean ± std** | **Mean ± std** | **Mean ± std** |
| MBT | 3.17 ± 0.90 | 5.47 ± 2.65 | 4.02 ± 1.54 | 11.47 ± 5.47 | 12.54 ± 7.06 |
| Affine | 3.97 ± 1.83 | 6.57 ± 3.46 | 3.19 ± 1.19 | 11.89 ± 5.66 | 12.41 ± 6.62 |
| 100 | 3.35 ± 1.19 | 4.76 ± 2.77 | 3.57 ± 0.99 | 10.83 ± 5.93 | 8.91 ± 6.76 |
| 500 | 3.46 ± 1.43 | 4.65 ± 2.73 | 3.72 ± 0.97 | 10.69 ± 5.99 | 7.95 ± 6.54 |
| 1,000 | 3.49 ± 1.53 | 4.64 ± 2.75 | 3.81 ± 0.96 | 10.62 ± 6.08 | 7.56 ± 6.39 |
| 2,000 | 3.54 ± 1.77 | 4.65 ± 2.82 | 3.88 ± 0.96 | 10.58 ± 6.17 | 7.24 ± 6.23 |

**TABLE 4 |** Geometric results compared to ANTs.

| Organs | Tools | DSC | MSD (mm) | 95%HD (mm) |
|---|---|---|---|---|
| | ANTs | 0.85 ± 0.08 | 1.72 ± 0.87 | 4.12 ± 1.92 |
| Prostate | `elastix` | **0.87 ± 0.05** | **1.42 ± 0.48** | **3.35 ± 1.19** |
| | ANTs | 0.48 ± 0.25 | 3.07 ± 1.87 | 6.76 ± 3.53 |
| Seminal vesicles | `elastix` | **0.63 ± 0.18** | **1.97 ± 1.22** | **4.76 ± 2.77** |
| | ANTs | 0.90 ± 0.04 | **1.33 ± 0.48** | **3.24 ± 1.20** |
| Lymph nodes | `elastix` | 0.89 ± 0.03 | 1.46 ± 0.44 | 3.57 ± 0.99 |
| | ANTs | 0.71 ± 0.08 | 4.01 ± 1.47 | 11.99 ± 5.61 |
| Rectum | `elastix` | **0.76 ± 0.06** | **3.29 ± 1.31** | **10.83 ± 5.93** |
| | ANTs | 0.78 ± 0.09 | 4.56 ± 2.14 | 12.63 ± 6.65 |
| Bladder | `elastix` | **0.86 ± 0.09** | **2.92 ± 1.90** | **8.91 ± 6.76** |

*For `elastix`, the results of 100 iteration for B-spline registration are reported. The bold value means the best results achieved by each method.*

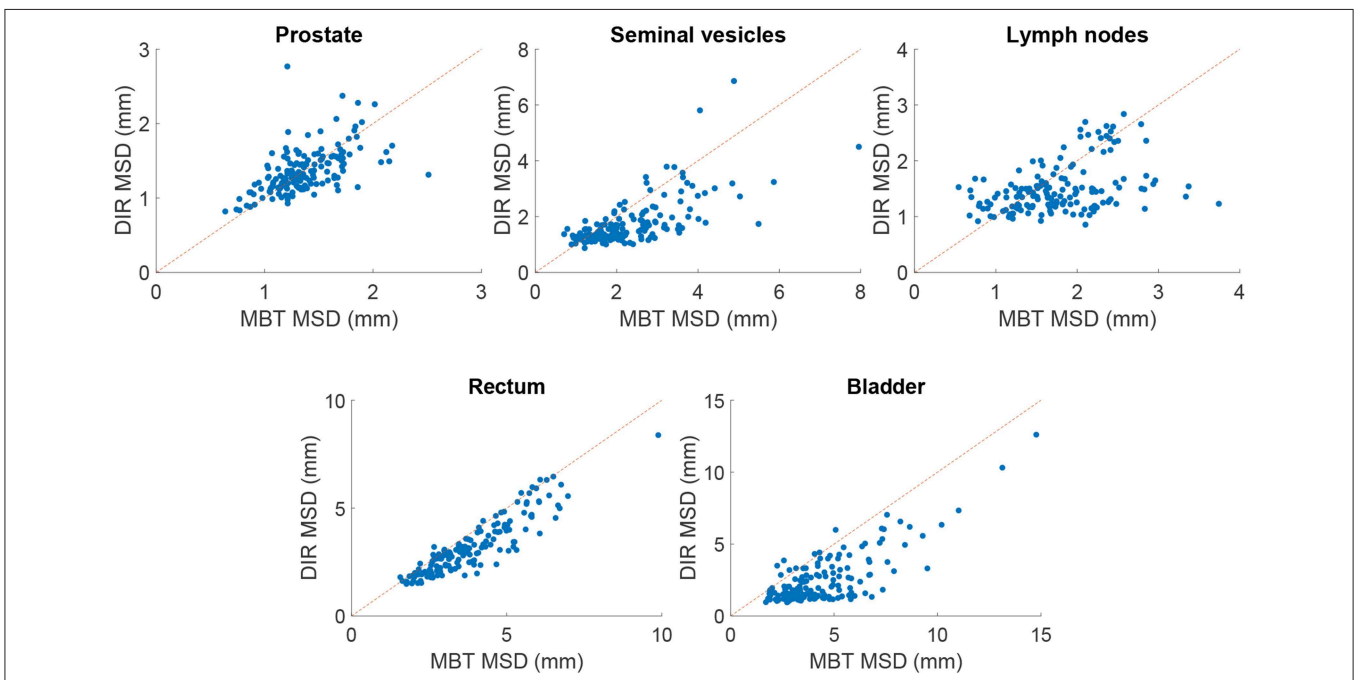


**FIGURE 2 |** Scatter plot of the MSD in mm of `elastix` DIR with 100 iterations compared with the results of MBT. The red line indicates the line of no change, i.e., points below this line indicate improvement of DIR over MBT.

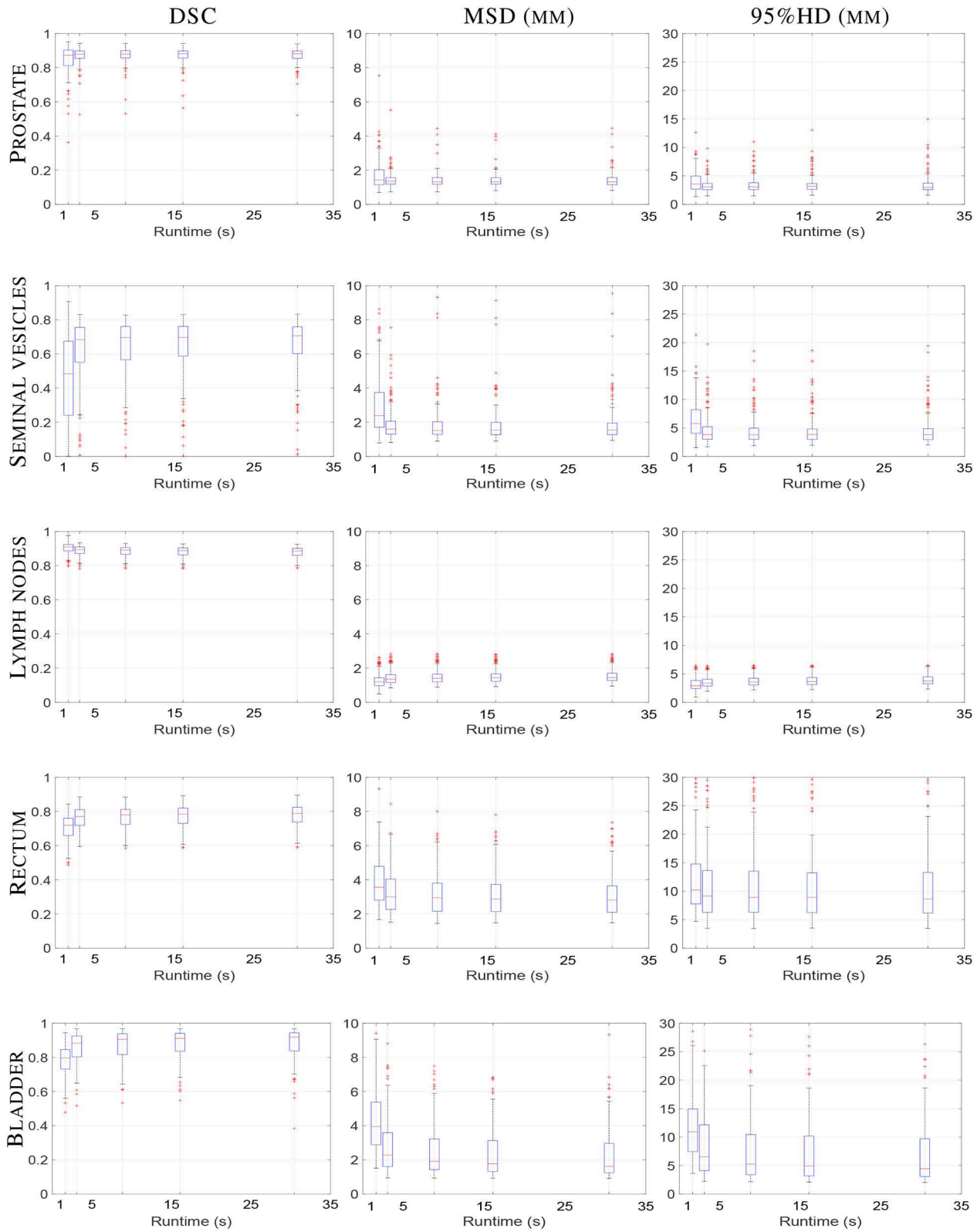


**FIGURE 3 |** Boxplot of `elastix` registration performance against runtime in seconds. From left column to right column the DSC (unit-less), MSD (mm) and 95%HD (mm) are shown, respectively. From top to bottom the prostate, seminal vesicles, lymph nodes, rectum and bladder are shown, respectively. Within one boxplot, from left to right the affine registration and B-spline registrations with 100, 500, 1,000, and 2,000 iterations are shown, respectively. Each boxplot contains results of 159 registrations.

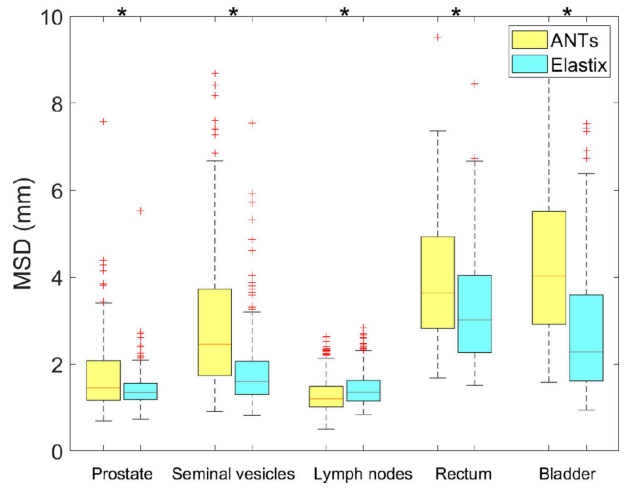


**FIGURE 4 |** Boxplot of MSD from `elastix` DIR 100 iterations compared to ANTs for different organs. Star above boxes means a statistical difference of a Wilcoxon signed-rank test between the two methods.

iterations over MBT in terms of dosimetric coverage. The 10 cases that did not directly meet our definition of clinical success had a $V_{95\%}$ for the prostate between 90% and 97% with a mean of 95% for DIR using 100 iterations, while for DIR using 500 iterations this range was between 93% and 97% with a mean of 96%. More details are given in the Discussion. See **Figure 1** for an example.

## 4. DISCUSSION

The purpose of this study was to investigate if automatic recontouring for prostate cancer IMPT would be possible, considering the clinical requirements for accuracy, robustness and speed. The overall goal of online adaptive IMPT is to be able to treat with a small margin (in this study 2 mm for the prostate and 3.5 mm for the seminal vesicles and lymph nodes) to spare OARs. This can only be done by daily re-planning, otherwise coverage loss or underdosage may occur, which is unacceptable. Such daily re-planning warrants automatic recontouring, in this study by DIR. To quantify the dosimetric impact of such re-planning, we not only performed a geometric validation but moreover a dosimetric validation, to assess the imperfections of automatic recontouring in terms of the clinically more relevant dose coverage. The chosen endpoint of our validation is therefore $V_{95\%} \geq 98\%$ for each of the target volumes. In general, the registration package `elastix` can automatically re-contour repeat CT scans of the prostate with a desirable accuracy in 3 s in 68.8% of cases. This compares favorably with MBT, which only obtained a success rate of 50%. `elastix` outperformed ANTs in this use case, in terms of registration accuracy as well as runtime efficiency. The parameter settings of ANTs were taken from Cao et al. (44), and then tuned with some efforts on a subset of the data. It may be that settings can be found that yield better registration accuracy, as the tuning was not exhaustive. Due to the nature of the ANTs algorithm, runtime performance however is highly in favor of `elastix`, an important aspect in online adaptive IMPT.

Several aspects were important for registration performance: (1) A correct initialization of the registration was found to be important to obtain desired accuracies. Alignment of bony anatomy, as used in this study, yielded satisfactory results (1, 52), but exploitation of the implanted gold markers could also be an option (50); (2) The couch is disturbing the registration and should therefore be removed by masking or cropping. In this study both were used, where cropping was also beneficial for runtime performance; (3) We observed performance differences when increasing the number of iterations, however, the effects are quite small, a few tenth of a millimeter. For example, the DSC of the lymph nodes decreased somewhat with increasing the number of iterations while the DSC of other organs increased, which may be caused by the deformation of the bladder which affected the lymph node region as well, see **Table 1**. (4) As we had compared the registration accuracy with and without mask, we found that masking is helpful for small volume organs such as the seminal vesicles and rectum, while no differences were observed for the prostate and lymph nodes. This finding is consistent with previous studies (1, 10).

In this study special attention was given to the registration runtime in relation to achieved accuracy, determined by the number of iterations used by DIR. Overall, registration accuracy increased only slightly when gradually increasing the number of iterations from 100 to 2000, suggesting that convergence was in most cases obtained already at 100 iterations. Only for the seminal vesicles an improvement in dose coverage was observed when using 500 iterations, see **Table 5**. The geometrical success rate as expressed by the percentage of registrations with an MSD below the slice thickness of 2 mm was 96% for the prostate. Clinical success rate, expressed by the dose coverage criteria, was 89% for the prostate. This means that in a high percentage of cases the automatically generated contours can be directly used for online adaptive IMPT, without the need for more time-consuming interaction. For those patients, smaller margins can be used and less robustness can be included than when using conventional non-adaptive planning [typically 7 mm margins (3, 49, 50)], resulting in less dose for the OARs and potentially less complications for the patients. For the remaining cases interaction is warranted, for example by manually supplying corresponding points at anatomical regions that require improvement (53, 54).

From the 93 registrations that were assessed in terms of target coverage, 10 did not directly meet the dose conformity constraints for the prostate. These cases were inspected visually, and we found that 2 cases had many gas pockets in the rectum, while for the other 8 cases no apparent reason was found. Note that no rectal balloon or SpaceOAR hydrogel was used for the current study. For cases with many gas pockets we may consider specialized DIR methodology using an intensity modification technique (55). The MSD of these two cases was around 2.3 mm, and therefore also did not meet the geometrical criteria. Of the 8 remaining cases, one case had a $V_{95\%}$ of 97.99%, which increased to $>$ 98% when 500 or

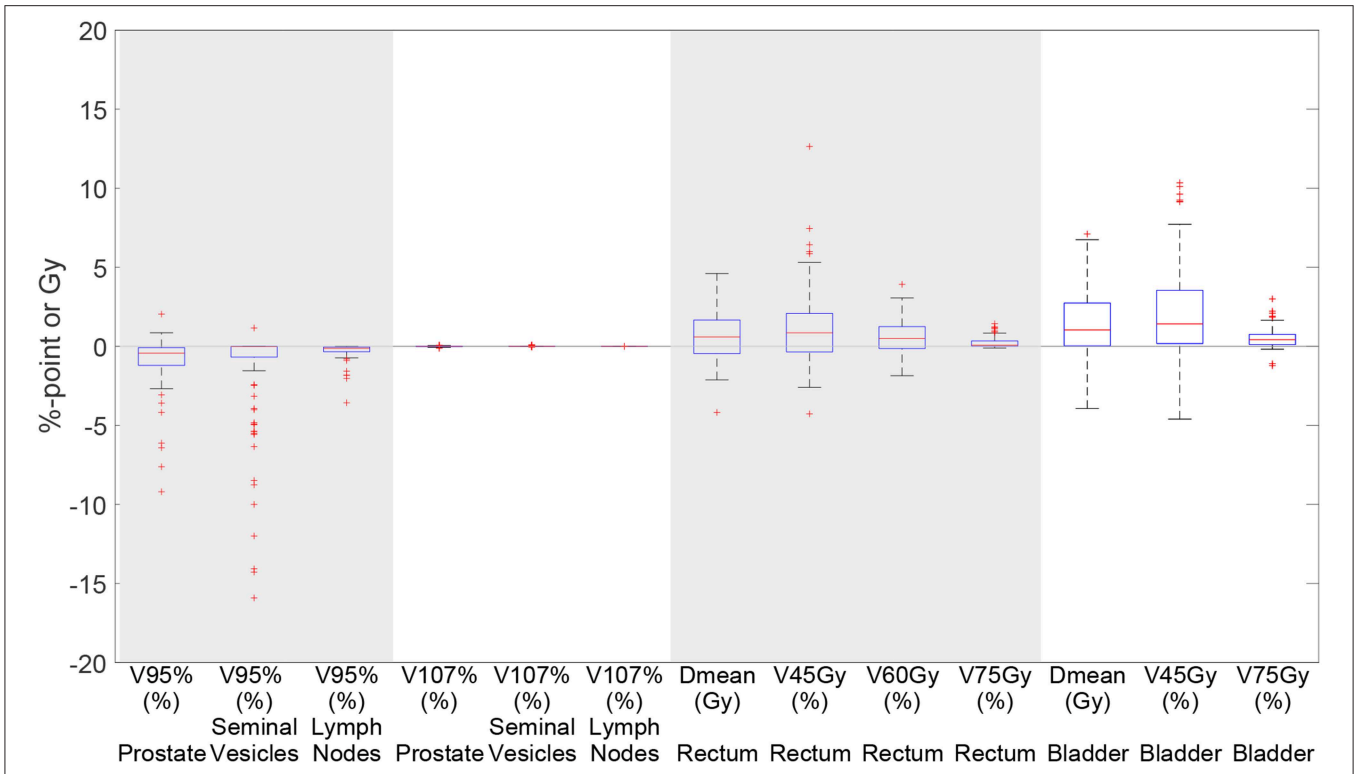


**FIGURE 5 |** Boxplot depicting the difference in dosimetric parameters between the automatically generated delineations and the manual delineations in the treatment plan based on the automatically generated delineations using `elastix` 100 iterations for 93 scans. Each box plot indicates the median and the 25th and 75th percentiles of the obtained differences. The line depicts the remaining differences which are not outliers. Values are defined outliers if they are more than 1.5 times the distance between the 25th and 75th quartiles away from the quartiles. The red marks indicate the outliers.

**TABLE 5 |** Percentage of `elastix` registrations that meet the dose constraints for the different contours.

| | $V_{95\%} \geq 98\%$ | | | | $V_{107\%} \leq 2\%$ | | |
|---|---|---|---|---|---|---|---|
| | **Prostate** | **Seminal vesicles** | **Lymph nodes** | **CSR** | **Prostate** | **Seminal vesicles** | **Lymph nodes** |
| MBT | 81.5 | 62.0 | 90.2 | 50.0 | 100.0 | 100.0 | 100.0 |
| 100 | 89.2 | 78.5 | 97.9 | 68.8 | 100.0 | 100.0 | 100.0 |
| 500 | 89.2 | 88.2 | 97.9 | 77.4 | 100.0 | 100.0 | 100.0 |
| 1,000 | 89.2 | 88.2 | 98.9 | 78.5 | 100.0 | 100.0 | 100.0 |
| 2,000 | 90.3 | 88.2 | 97.9 | 77.4 | 100.0 | 100.0 | 100.0 |

*Conservative success rate (CSR) refers to the percentage of registrations for which all target volumes (the prostate, seminal vesicles and lymph nodes) meet the dose constraints.*

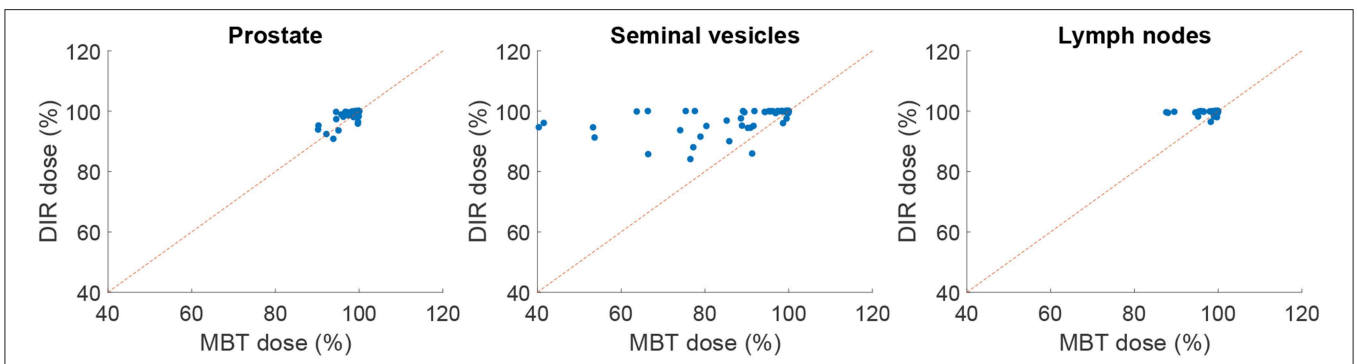


**FIGURE 6 |** Scatter plot comparing `elastix` DIR (100 iterations) with MBT, in terms of dosimetric coverage ($V_{95\%}$). The red line indicates the line of no change, i.e., points above this line indicate improvement of DIR over MBT.

more iterations were used. Two cases had a $V_{95\%}$ around 97% for all settings, which is very close the threshold of 98%; both had an MSD of 1.3 mm, meeting the geometrical criterion for success. Two cases had a $V_{95\%}$ of 96%, which improved to 98% and 99% when 500 iterations or more were used. The remaining three cases obtained a $V_{95\%}$ in the range 92–96% for the prostate and an MSD in the range 1.6-1.8 mm, so were not far from success.

In order to use the open source package `elastix` in a clinical setting, several aspects should be considered. Although the runtime of DIR is reduced to seconds in the current study, other steps in the entire replanning process should also be considered to shorten the procedure and improve the quality. Special attention should be paid to the intrafraction motion of the CTV between the time of CT image acquisition and the planned dose treatment delivery (56, 57). For online adaptive IMPT, one could use the daily imaging techniques, such as CT and MR, to obtain the new position of hard or soft tissues. They can also use the implanted fiducial markers, rectal balloon or SpaceOAR hydrogel to guide the new treatment delivery (22, 58–64). All of these require a reasonable margin to tackle the randomness of the intrafraction motion of the CTV. With the help of reduced registration time, even smaller margins (less than 2 or 1 mm) could be possible (65) and other uncertainties are under control. Quality control is another important issue, which can be performed via visual inspection of the generated contours, but assistance by automatic techniques for uncertainty estimation of image registration may be of interest (66, 67). These techniques may pinpoint areas of possible misregistration, thus enabling a quicker assessment of registration quality. Contours generated by `elastix` could be directly used in 89% of cases, meaning that for 11% of cases manual assistance or fall-back strategies are needed. Registration can for example be efficiently improved by manually indicating a few landmarks on segmentation boundaries (54). Robustness may be further improved by taking into account automatic estimates of the bladder (68) in the registration by optimizing a joint functional. In this study we used clinical quality repeat CT scans, which assumes the availability of an in-room CT-on-rails system (69–71). Since such a system is not available in all hospitals, alternatively Cone Beam CT (CBCT) may be used in-room (20, 72). However, the reduced soft-tissue contrast of CBCT images may increase the uncertainty of DIR, which therefore may influence the quality of the IMPT plans. Lastly, the registration time assessed in this paper is determined by the number of iterations, which is not case-specific (36, 73). For cases that are geometrically close, DIR may finish the task with less than 100 iterations, while for difficult cases the number of iterations may be much larger. An adaptive stopping condition for stochastic gradient descent, such as considering a moving average of the noisy cost function values (or gradient), may remedy this. Moreover, a further reduction in runtime may be obtained with the help of a graphics processing unit (GPU) and other computational techniques (11, 74–76).

## 5. CONCLUSION

In this study we showed that the open source registration package `elastix` can automatically re-contour repeat CT scans of the prostate in 3 s, yielding treatment plans that directly meet the dose conformity constraints in 78.5–97.9% of cases, and a geometrical criteria of success in 96% of cases. This software may therefore facilitate online adaptive proton therapy of prostate cancer, enabling a reduction in treatment margins and robustness that needs to be included in the treatment plan.

## DATA AVAILABILITY STATEMENT

The CT-data with contours were collected at Haukeland University Hospital, Bergen, Norway and were provided to us by responsible oncologist Svein Inge Helle and physicist Liv Bolstad Hysing. Requests to access this dataset should be directed to Liv Bolstad Hysing, liv.bolstad.hysing@helse-bergen.no.

## ETHICS STATEMENT

The trial had been approved by the local ethical committee of REC West, the western Norway regional committee for medical and health research ethics (number 2006-15727). Written informed consent was obtained for participation in the study.

## AUTHOR CONTRIBUTIONS

YQ contributed to experimental design, implementation, geometric evaluation, interpretation of the data, and the writing of the manuscript. TJ contributed to the implementation, experiments on dosimetric evaluation, and interpretation of the data. MH, BL, and MS were involved in experimental design, in the writing of the manuscript, and have read and approved the final version.

## FUNDING

This study was financially supported by ZonMw, the Netherlands Organization for Health Research and Development, grant number 104003012 and by Varian Medical Systems, and by the China Scholarship Council (No. 201206130066).

## ACKNOWLEDGMENTS

Erasmus MC Cancer Institute also has research collaborations with Elekta AB, Stockholm, Sweden and Accuray Inc., Sunnyvale, USA. The CT-data with contours were collected at Haukeland University Hospital, Bergen, Norway and were provided to us by responsible oncologist Svein Inge Helle and physicist Liv Bolstad Hysing; they are gratefully acknowledged.

## REFERENCES


1. Thörnqvist S, Petersen JBB, Høyer M, Bentzen LN, Muren LP. Propagation of target and organ at risk contours in radiotherapy of prostate cancer using deformable image registration. *Acta Oncol.* (2010) 49:1023–32. doi: 10.3109/0284186X.2010.503662
2. Zhang M, Westerly D, Mackie T. Introducing an on-line adaptive procedure for prostate image guided intensity modulate proton therapy. *Phys Med Biol.* (2011) 56:4947. doi: 10.1088/0031-9155/56/15/019
3. Thörnqvist S, Muren LP, Bentzen L, Hysing LB, Høyer M, Grau C, et al. Degradation of target coverage due to inter-fraction motion during intensity-modulated proton therapy of prostate and elective targets. *Acta Oncol.* (2013) 52:521–7. doi: 10.3109/0284186X.2012.752860
4. Lomax A. Intensity modulated proton therapy and its sensitivity to treatment uncertainties 1: the potential effects of calculational uncertainties. *Phys Med Biol.* (2008) 53:1027. doi: 10.1088/0031-9155/53/4/014
5. Lomax A. Intensity modulated proton therapy and its sensitivity to treatment uncertainties 2: the potential effects of inter-fraction and inter-field motions. *Phys Med Biol.* (2008) 53:1043. doi: 10.1088/0031-9155/53/4/015
6. Brock KK, Mutic S, McNutt TR, Li H, Kessler ML. Use of image registration and fusion algorithms and techniques in radiotherapy: report of the AAPM radiation therapy committee task group no. 132. *Med Phys.* (2017) 44:e43–76. doi: 10.1002/mp.12256
7. Xing L, Siebers J, Keall P. Computational challenges for image-guided radiation therapy: framework and current research. *Semin Radiat Oncol.* (2007). 17:245–57. doi: 10.1016/j.semradonc.2007.07.004
8. Castadot P, Lee JA, Parraga A, Geets X, Macq B, Grégoire V. Comparison of 12 deformable registration strategies in adaptive radiation therapy for the treatment of head and neck tumors. *Radiother Oncol.* (2008) 89:1–12. doi: 10.1016/j.radonc.2008.04.010
9. Wognum S, Heethuis S, Rosario T, Hoogeman M, Bel A. Validation of deformable image registration algorithms on CT images of *ex vivo* porcine bladders with fiducial markers. *Med Phys.* (2014) 41:071916. doi: 10.1118/1.4883839
10. Kumarasiri A, Siddiqui F, Liu C, Yechieli R, Shah M, Pradhan D, et al. Deformable image registration based automatic CT-to-CT contour propagation for head and neck adaptive radiotherapy in the routine clinical setting. *Med Phys.* (2014) 41:121712. doi: 10.1118/1.4901409
11. Shackleford JA, Kandasamy N, Sharp G. On developing B-spline registration algorithms for multi-core processors. *Phys Med Biol.* (2010) 55:6329. doi: 10.1088/0031-9155/55/21/001
12. Klein S, Staring M, Murphy K, Viergever MA, Pluim JPW. Elastix: a toolbox for intensity-based medical image registration. *IEEE Trans Med Imaging.* (2010) 29:196–205. doi: 10.1109/TMI.2009.2035616
13. Yang D, Brame S, El Naqa I, Aditya A, Wu Y, Murty Goddu S, et al. DIRART–A software suite for deformable image registration and adaptive radiotherapy research. *Med Phys.* (2011) 38:67–77. doi: 10.1118/1.3521468
14. Ince DC, Hatton L, Graham-Cumming J. The case for open computer programs. *Nature.* (2012) 482:485–88. doi: 10.1038/nature10836
15. Lowekamp BC, Chen DT, Ibáñez L, Blezek D. The design of SimpleITK. *Front Neuroinform.* (2013) 7:45. doi: 10.3389/fninf.2013.00045
16. Thor M, Andersen ES, Petersen JB, Sørensen TS, Noe KØ, Tanderup K, et al. Evaluation of an application for intensity-based deformable image registration and dose accumulation in radiotherapy. *Acta Oncol.* (2014) 53:1329–36. doi: 10.3109/0284186X.2014.928742
17. Cazoulat G, Simon A, Dumenil A, Gnep K, De Crevoisier R, Acosta O, et al. Surface-constrained nonrigid registration for dose monitoring in prostate cancer radiotherapy. *IEEE Trans Med Imaging.* (2014) 33:1464–74. doi: 10.1109/TMI.2014.2314574
18. Nassef M, Simon A, Cazoulat G, Duménil A, Blay C, Lafond C, et al. Quantification of dose uncertainties in cumulated dose estimation compared to planned dose in prostate IMRT. *Radiother Oncol.* (2016) 119:129–36. doi: 10.1016/j.radonc.2016.03.007
19. Zhang T, Chi Y, Meldolesi E, Yan D. Automatic delineation of on-line head-and-neck computed tomography images: toward on-line adaptive radiotherapy. *Int J Radiat Oncol Biol Phys.* (2007) 68:522–30. doi: 10.1016/j.ijrobp.2007.01.038
20. Landry G, Nijhuis R, Dedes G, Handrack J, Thieke C, Janssens G, et al. Investigating CT to CBCT image registration for head and neck proton therapy as a tool for daily dose recalculation. *Med Phys.* (2015) 42:1354–66. doi: 10.1118/1.4908223
21. Castadot P, Geets X, Lee JA, Christian N, Grégoire V. Assessment by a deformable registration method of the volumetric and positional changes of target volumes and organs at risk in pharyngo-laryngeal tumors treated with concomitant chemo-radiation. *Radiother Oncol.* (2010) 95:209–17. doi: 10.1016/j.radonc.2010.03.007
22. Kupelian P, Willoughby T, Mahadevan A, Djemil T, Weinstein G, Jani S, et al. Multi-institutional clinical experience with the Calypso System in localization and continuous, real-time monitoring of the prostate gland during external radiotherapy. *Int J Radiat Oncol Biol Phys.* (2007) 67:1088–98. doi: 10.1016/j.ijrobp.2006.10.026
23. van der Wielen GJ, Mutanga TF, Incrocci L, Kirkels WJ, Osorio EMV, Hoogeman MS, et al. Deformation of prostate and seminal vesicles relative to intraprostatic fiducial markers. *Int J Radiat Oncol Biol Phys.* (2008) 72:1604–11. doi: 10.1016/j.ijrobp.2008.07.023
24. Thörnqvist S, Hysing LB, Zolnay AG, Söhn M, Hoogeman MS, Muren LP, et al. Treatment simulations with a statistical deformable motion model to evaluate margins for multiple targets in radiotherapy for high-risk prostate cancer. *Radiother Oncol.* (2013) 109:344–9. doi: 10.1016/j.radonc.2013.09.012
25. Ariyaratne H, Chesham H, Pettingell J, Alonzi R. Image-guided radiotherapy for prostate cancer with cone beam CT: dosimetric effects of imaging frequency and PTV margin. *Radiother Oncol.* (2016) 121:103–8. doi: 10.1016/j.radonc.2016.07.018
26. Godley A, Ahunbay E, Peng C, Li XA. Automated registration of large deformations for adaptive radiation therapy of prostate cancer. *Med Phys.* (2009) 36:1433–41. doi: 10.1118/1.3095777
27. Li W, Jaffray DA, Wilson G, Moseley D. How long does it take? An analysis of volumetric image assessment time. *Radiother Oncol.* (2016) 119:150–3. doi: 10.1016/j.radonc.2016.01.015
28. Liu C, Kim J, Kumarasiri A, Mayyas E, Brown SL, Wen N, et al. An automated dose tracking system for adaptive radiation therapy. *Comput Methods Prog Biomed.* (2018) 154:1–8. doi: 10.1016/j.cmpb.2017.11.001
29. Lamb J, Cao M, Kishan A, Agazaryan N, Thomas DH, Shaverdian N, et al. Online adaptive radiation therapy: implementation of a new process of care. *Cureus.* (2017) 9:e1618. doi: 10.7759/cureus.1618
30. de Vos BD, Wolterink JM, de Jong PA, Leiner T, Viergever MA, Išgum I. ConvNet-based localization of anatomical structures in 3-D medical images. *IEEE Trans Med Imaging.* (2017) 36:1470–81. doi: 10.1109/TMI.2017.2673121
31. Sokooti H, de Vos B, Berendsen F, Lelieveldt BP, Išgum I, Staring M. Nonrigid image registration using multi-scale 3D convolutional neural networks. In: *International Conference on Medical Image Computing and Computer-Assisted Intervention*. Quebec City, QC: Springer (2017). p. 232–9.
32. de Vos BD, Berendsen FF, Viergever MA, Sokooti H, Staring M, Išgum I. A deep learning framework for unsupervised affine and deformable image registration. *Med Image Anal.* (2019) 52:128–43. doi: 10.1016/j.media.2018.11.010
33. Avants BB, Tustison N, Song G. Advanced normalization tools (ANTS). *Insight J.* (2009) 2:1–35. Available online at: http://hdl.handle.net/10380/3113
34. Muren LP, Wasbø E, Helle SI, Hysing LB, Karlsdottir À, Odland OH, et al. Intensity-modulated radiotherapy of pelvic lymph nodes in locally advanced prostate cancer: planning procedures and early experiences. *Int J Radiat Oncol Biol Phys.* (2008) 71:1034–41. doi: 10.1016/j.ijrobp.2007.11.060
35. Staring M, Bakker M, Stolk J, Shamonin D, Reiber J, Stoel B. Towards local progression estimation of pulmonary emphysema using CT. *Med Phys.* (2014) 41:021905. doi: 10.1118/1.4851535
36. Qiao Y, van Lew B, Lelieveldt BP, Staring M. Fast automatic step size estimation for gradient descent optimization of image registration. *IEEE Trans Med Imaging.* (2015) 35:391–403. doi: 10.1109/TMI.2015.2476354
37. Rueckert D, Sonoda LI, Hayes C, Hill DL, Leach MO, Hawkes DJ. Nonrigid registration using free-form deformations: application to breast MR images. *IEEE Trans Med Imaging.* (1999) 18:712–21. doi: 10.1109/42.796284

38. Huizinga W, Klein S, Poot DHJ. Fast multidimensional B-spline interpolation using template metaprogramming. In: *Lecture Notes in Computer Science (including subseries Lecture Notes in Artificial Intelligence and Lecture Notes in Bioinformatics)* London, UK: WBIR 2014 (2014).
39. Thévenaz P, Unser M. Optimization of mutual information for multiresolution image registration. *IEEE Trans Image Process*. (2000) 9:2083–99. doi: 10.1109/83.887976
40. Tustison NJ, Cook PA, Klein A, Song G, Das SR, Duda JT, et al. Large-scale evaluation of ANTs and FreeSurfer cortical thickness measurements. *Neuroimage*. (2014) 99:166–79. doi: 10.1016/j.neuroimage.2014.05.044
41. Murphy K, van Ginneken B, Reinhardt JM, Kabus S, Ding K, Deng X, et al. Evaluation of registration methods on thoracic CT: the EMPIRE10 challenge. *IEEE Trans Med Imaging*. (2011) 30:1901–20. doi: 10.1109/TMI.2011.2158349
42. Wang P, Yin L, Zhang Y, Kirk M, Song G, Ahn PH, et al. Quantitative assessment of anatomical change using a virtual proton depth radiograph for adaptive head and neck proton therapy. *J Appl Clin Med Phys*. (2016) 17:427–40. doi: 10.1120/jacmp.v17i2.5819
43. Moding EJ, Clark DP, Qi Y, Li Y, Ma Y, Ghaghada K, et al. Dual-energy micro-computed tomography imaging of radiation-induced vascular changes in primary mouse sarcomas. *Int J Radiat Oncol Biol Phys*. (2013) 85:1353–9. doi: 10.1016/j.ijrobp.2012.09.027
44. Cao X, Gao Y, Yang J, Wu G, Shen D. Learning-based multimodal image registration for prostate cancer radiation therapy. In: *International Conference on Medical Image Computing and Computer-Assisted Intervention*. Athens: Springer (2016). p. 1–9.
45. Klein A, Andersson J, Ardekani BA, Ashburner J, Avants B, Chiang MC, et al. Evaluation of 14 nonlinear deformation algorithms applied to human brain MRI registration. *NeuroImage*. (2009) 46:786–802. doi: 10.1016/j.neuroimage.2008.12.037
46. Lu C, Chelikani S, Papademetris X, Knisely JP, Milosevic MF, Chen Z, et al. An integrated approach to segmentation and nonrigid registration for application in image-guided pelvic radiotherapy. *Med Image Anal*. (2011) 15:772–85. doi: 10.1016/j.media.2011.05.010
47. Breedveld S, Storchi PR, Voet PW, Heijmen BJ. iCycle: integrated, multicriterial beam angle, and profile optimization for generation of coplanar and noncoplanar IMRT plans. *Med Phys*. (2012) 39:951–63. doi: 10.1118/1.3676689
48. Van de Water S, Kraan A, Breedveld S, Schillemans W, Teguh D, Kooy H, et al. Improved efficiency of multi-criteria IMPT treatment planning using iterative resampling of randomly placed pencil beams. *Phys Med Biol*. (2013) 58:6969. doi: 10.1088/0031-9155/58/19/6969
49. Moteabbed M, Trofimov A, Sharp G, Wang Y, Zietman A, Efstathiou J, et al. Proton therapy of prostate cancer by anterior-oblique beams: implications of setup and anatomy variations. *Phys Med Biol*. (2017) 62:1644. doi: 10.1088/1361-6560/62/5/1644
50. Thörnqvist S, Bentzen L, Petersen JBB, Hysing LB, Muren LP. Plan robustness of simultaneous integrated boost radiotherapy of prostate and lymph nodes for different image-guidance and delivery techniques. *Acta Oncol*. (2011) 50:926–34. doi: 10.3109/0284186X.2011.590522
51. Jagt T, Breedveld S, Van de Water S, Heijmen B, Hoogeman M. Near real-time automated dose restoration in IMPT to compensate for daily tissue density variations in prostate cancer. *Phys Med Biol*. (2017) 62:4254. doi: 10.1088/1361-6560/aa5c12
52. Bondar L, Hoogeman M, Mens JW, Dhawtal G, De Pree I, Ahmad R, et al. Toward an individualized target motion management for IMRT of cervical cancer based on model-predicted cervix–uterus shape and position. *Radiother Oncol*. (2011) 99:240–5. doi: 10.1016/j.radonc.2011.03.013
53. Qin A, Sun Y, Liang J, Yan D. Evaluation of online/offline image guidance/adaptation approaches for prostate cancer radiation therapy. *Int J Radiat Oncol Biol Phys*. (2015) 91:1026–33. doi: 10.1016/j.ijrobp.2014.12.043
54. Gunay G, Ha LM, van Walsum T, Klein S. Semi-automated registration of pre-and intra-operative liver CT for image-guided interventions. In: *Medical Imaging 2016: Image Processing. vol. 9784. International Society for Optics and Photonics*. San Diego, CA (2016). p. 97841N.
55. Gao S, Zhang L, Wang H, De Crevoisier R, Kuban DD, Mohan R, et al. A deformable image registration method to handle distended rectums in prostate cancer radiotherapy. *Med Phys*. (2006) 33:3304–12. doi: 10.1118/1.2222077
56. Kotte ANTJ, Hofman P, Lagendijk JJW, van Vulpen M, van der Heide UA. Intrafraction motion of the prostate during external-beam radiation therapy: analysis of 427 patients with implanted fiducial markers. *Int J Radiat Oncol Biol Phys*. (2007) 69:419–25. doi: 10.1016/j.ijrobp.2007.03.029
57. Litzenberg DW, Balter JM, Hadley SW, Sandler HM, Willoughby TR, Kupelian PA, et al. Influence of intrafraction motion on margins for prostate radiotherapy. *Int J Radiat Oncol Biol Phys*. (2006) 65:548–53. doi: 10.1016/j.ijrobp.2005.12.033
58. Wang KKH, Vapiwala N, Deville C, Plastaras JP, Scheuermann R, Lin H, et al. A study to quantify the effectiveness of daily endorectal balloon for prostate intrafraction motion management. *Int J Radiat Oncol Biol Phys*. (2012) 83:1055–63. doi: 10.1016/j.ijrobp.2011.07.038
59. Both S, Wang KKH, Plastaras JP, Deville C, Bar Ad V, Tochner Z, et al. Real-time study of prostate intrafraction motion during external beam radiotherapy with daily endorectal balloon. *Int J Radiat Oncol Biol Phys*. (2011) 81:1302–9. doi: 10.1016/j.ijrobp.2010.08.052
60. Smeenk RJ, Louwe RJW, Langen KM, Shah AP, Kupelian PA, Van Lin ENJT, et al. An endorectal balloon reduces intrafraction prostate motion during radiotherapy. *Int J Radiat Oncol Biol Phys*. (2012) 83:661–9. doi: 10.1016/j.ijrobp.2011.07.028
61. Kupelian PA, Langen KM, Willoughby TR, Zeidan OA, Meeks SL. Image-guided radiotherapy for localized prostate cancer: treating a moving target. *Semin Radiat Oncol*. (2008) 18:58–66. doi: 10.1016/j.semradonc.2007.09.008
62. Whalley D, Hruby G, Alfieri F, Kneebone A, Eade T. SpaceOAR hydrogel in dose-escalated prostate cancer radiotherapy: rectal dosimetry and late toxicity. *Clin Oncol*. (2016) 28:e148–54. doi: 10.1016/j.clon.2016.05.005
63. Strom TJ, Wilder RB, Fernandez DC, Mellon EA, Saini AS, Hunt DC, et al. A dosimetric study of polyethylene glycol hydrogel in 200 prostate cancer patients treated with high-dose rate brachytherapy ± intensity modulated radiation therapy. *Radiother Oncol*. (2014) 111:126–31. doi: 10.1016/j.radonc.2014.02.011
64. Lambert J, Greer PB, Menk F, Patterson J, Parker J, Dahl K, et al. MRI-guided prostate radiation therapy planning: investigation of dosimetric accuracy of MRI-based dose planning. *Radiother Oncol*. (2011) 98:330–4. doi: 10.1016/j.radonc.2011.01.012
65. Keall P, Poulsen P, Booth JT. See, think, and act: real-time adaptive radiotherapy. *Semin Radiat Oncol*. (2019) 29:228–35. doi: 10.1016/j.semradonc.2019.02.005
66. Saygili G, Staring M, Hendriks EA. Confidence estimation for medical image registration based on stereo confidences. *IEEE Trans Med Imaging*. (2015) 35:539–49. doi: 10.1109/TMI.2015.2481609
67. Sokooti H, Saygili G, Glocker B, Lelieveldt BP, Staring M. Accuracy estimation for medical image registration using regression forests. In: *International Conference on Medical Image Computing and Computer-Assisted Intervention*. Athens: Springer (2016). p. 107–15.
68. Cha KH, Hadjiiski L, Samala RK, Chan HP, Caoili EM, Cohan RH. Urinary bladder segmentation in CT urography using deep-learning convolutional neural network and level sets. *Med Phys*. (2016) 43:1882–96. doi: 10.1118/1.4944498
69. Timmerman RD, Xing L. *Image-Guided and Adaptive Radiation Therapy*. Lippincott Williams & Wilkins (2012).
70. Li X, Quan EM, Li Y, Pan X, Zhou Y, Wang X, et al. A fully automated method for CT-on-rails-guided online adaptive planning for prostate cancer intensity modulated radiation therapy. *Int J Radiat Oncol Biol Phys*. (2013) 86:835–41. doi: 10.1016/j.ijrobp.2013.04.014
71. Papalazarou C, Klop GJ, Milder MT, Marijnissen JP, Gupta V, Heijmen BJ, et al. CyberKnife with integrated CT-on-rails: system description and first clinical application for pancreas SBRT. *Med Phys*. (2017) 44:4816–27. doi: 10.1002/mp.12432

72. Veiga C, Janssens G, Teng CL, Baudier T, Hotoiu L, McClelland JR, et al. First clinical investigation of cone beam computed tomography and deformable registration for adaptive proton therapy for lung cancer. *Int J Radiat Oncol Biol Phys*. (2016) 95:549–59. doi: 10.1016/j.ijrobp.2016.01.055
73. Sun W, Poot DH, Smal I, Yang X, Niessen WJ, Klein S. Stochastic optimization with randomized smoothing for image registration. *Med Image Anal*. (2017) 35:146–58. doi: 10.1016/j.media.2016.07.003
74. Shamonin DP, Bron EE, Lelieveldt BP, Smits M, Klein S, Staring M. Fast parallel image registration on CPU and GPU for diagnostic classification of Alzheimer's disease. *Front Neuroinform*. (2014) 7:50. doi: 10.3389/fninf.2013.00050
75. Sharp G, Kandasamy N, Singh H, Folkert M. GPU-based streaming architectures for fast cone-beam CT image reconstruction and Demons deformable registration. *Phys Med Biol*. (2007) 52:5771. doi: 10.1088/0031-9155/52/19/003
76. Qiao Y, Lelieveldt BP, Staring M. An efficient preconditioner for stochastic gradient descent optimization of image registration. *IEEE Trans Med Imaging*. (2019) 38:2314–25. doi: 10.1109/TMI.2019.2897943

**Conflict of Interest:** TJ reports grants from Varian Medical Systems, Pao Alto, US, during the conduct of the study; grants from Elekta AB, Stockholm, Sweden, grants from Accuray, Sunnyvale, US, outside the submitted work. MH reports grants from Varian Medical Systems, Pao Alto, US, during the conduct of the study; grants from Elekta AB, Stockholm, Sweden, grants from Accuray, Sunnyvale, US, outside the submitted work.

The remaining authors declare that the research was conducted in the absence of any commercial or financial relationships that could be construed as a potential conflict of interest.